A LETTERS JOURNAL EXPLORING THE FRONTIERS OF PHYSICS

Società Italiana di Fisica

edp sciences

IOP Institute of Physics

LETTER

Mitigating hydrodynamic mix at the gas-ice interface with a combination of magnetic, ablative, and viscous stabilization

To cite this article: Bhuvana Srinivasan and Xian-Zhu Tang 2014 *EPL* **107** 65001

A LETTERS JOURNAL EXPLORING THE FRONTIERS OF PHYSICS

September 2014

EPL, **107** (2014) 65001
doi: 10.1209/0295-5075/107/65001

www.epljournal.org

Mitigating hydrodynamic mix at the gas-ice interface with a combination of magnetic, ablative, and viscous stabilization

BHUVANA SRINIVASAN[1,2] and XIAN-ZHU TANG[1]

[1] *Theoretical Division, Los Alamos National Laboratory - Los Alamos, NM 87545*
[2] *Department of Aerospace and Ocean Engineering, Virginia Tech - Blacksburg, VA 24061*

received 1 May 2014; accepted in final form 22 August 2014
published online 8 September 2014

PACS 52.57.Fg – Implosion symmetry and hydrodynamic instability (Rayleigh-Taylor, Richtmyer-Meshkov, imprint, etc.)
PACS 47.20.Ma – Interfacial instabilities (*e.g.*, Rayleigh-Taylor)
PACS 52.30.Ex – Two-fluid and multi-fluid plasmas

Abstract – Mix reduction is an important ingredient in yield performance in inertial confinement fusion (ICF). In an ignition-grade target design, shell adiabat shaping can mitigate hydrodynamic mix at the outer ablator surface via a high adiabat like that in the high-foot design, but the high Atwood number at the gas-ice interface associated with a low-adiabat ice, which is desirable for achieving high convergence ratio for a given laser system, still provides a robust drive for hydrodynamic instability during the deceleration phase of the implosion. The results presented here show that combined magnetic, viscous, and ablative stabilization can complement each other for adequate mix mitigation at the gas-ice interface in a range of magnetic-field strengths that are experimentally accessible.

The recent success of the high-foot campaign [1–3] on the National Ignition Facility (NIF) [4], especially in comparison with the conventional low-foot design [5,6], provides a concrete example that mix reduction holds a key to high performance in inertial confinement fusion (ICF) [7]. The stabilizing effect is attributed to the high adiabat of the pusher due to early heating by the increased laser power of the high-foot design. A high-adiabat pusher brings at least two stabilizing effects: the first is the stronger ablative stabilization of the outer pusher surface where hydrodynamic instabilities can feed through the pusher shell and subsequently seed the Rayleigh-Taylor instability (RTI) at the shell-gas interface; the second is a smaller Atwood number in comparison with that of a low-adiabat pusher which implies a weaker drive for RTI. A high-adiabat pusher does have the important trade-off of a reduced convergence ratio with a given laser system. Along this line, an immediate research focus is to demarcate the power threshold at which the highest convergence ratio can be achieved while still compatible with adequate mix reduction for high fusion yield. A promising approach is shell adiabat shaping [8], in which the outer layer of the pusher is designed to have a high adiabat while the bulk of the pusher/ice assembly (which, as a whole, is sometimes referred to as the shell for convenience) has a low adiabat. It can have greater ablative stabilization at the ablator outer surface due to a combination of high ablation speed and increased density gradient length scale, while retaining a large Atwood number at the gas-ice interface, which is still prone to RTI. Since mix reduction plays such an important role for ICF performance, a strategy to integrate the different mix mitigation schemes is crucial, especially for a high convergence design that necessarily retains a large Atwood number at the gas-ice interface. This is not only of fundamental physics interest, but also important to maximize the chance for ignition at the lowest laser energy.

The detrimental effect of hydrodynamic mix on ICF target performance is often explained in the following two ways. The first involves small amounts of pusher material, such as carbon, jetted into the gas core via hydrodynamic instabilities. The high-Z pusher materials can radiatively cool the gas core, preventing the formation of a hot-spot of sufficiently high ion temperature [9]. Radiation hydrodynamic simulations [10,11] suggest that these jets are of very high mode numbers. This type of mix is more generally known as the so-called chunk mix. The second concerns the heating of the inner shell materials, which in a cryogenic target is the fuel ice, into the hot spot via thermal conduction from the gas core. This is inevitable as the thermal conduction energy transfer across the interface of fuel ice and hot gas is given by

$$Q = \int_\Sigma (\kappa_e \nabla T_e + \kappa_i \nabla T_i) \cdot \mathrm{d}\mathbf{S} \approx \int_\Sigma \kappa_e \nabla T_e \cdot \mathrm{d}\mathbf{S}. \quad (1)$$

In the usual case where T_i is comparable to T_e, the conductive energy transfer from the hot spot is dominated by electron thermal conduction. Here Σ is the gas-ice interface area across which the energy exchange takes place, and $\kappa_{e,i}$ is the electron (ion) thermal conductivity across the interface. The amount of fuel ice that will be heated into the hot spot is directly proportional to Q integrated over implosion time. This results in a more massive but cooler hot spot, which tends to have a much inferior thermonuclear yield rate due to the strong T_i-dependence of DT fusion cross-section σ in the $T_i \in (1, 10)$ keV range. For comparable ∇T_e, the mass gain in the hot-spot is linearly proportional to the interface area Σ. The spherically symmetric implosion sets the absolute minimum $\Sigma_0 = 4\pi R^2$ with R the radius of the gas-ice interface. Hydrodynamic mix at the gas-ice interface, which is dominated by the so-called interfacial mix that can produce a much enlarged hot-spot perimeter, can drastically promote hot-spot energy loss and heating of the ice into the hot spot for $\Sigma \gg \Sigma_0$.

A higher yield performance thus requires that mix be effectively mitigated so Σ does not grow to be much larger than Σ_0. Success in controlling Σ often implies a reduction in the jetting of high-Z pusher materials into the gas core, since the jets are due to extremely short-wavelength modes, they would be most amendable to the various stabilization mechanisms. The most well-known stabilizing effect is due to the ablation of fuel ice into the gas core [12,13]. In other words, the very process of mass gain in the hot spot due to its heat loss tends to counteract the RTI that can aggravate the hot-spot energy loss and mass gain. A less well-known but increasingly recognized stabilizing effect is the hot-spot ion viscosity, which can be very large as the hot-spot ions reach multi-keV temperatures since the ion viscosity scales as $T_i^{5/2}$. The disparate temperature/viscosity profile across the gas-ice interface results in an inviscid, high-density fluid (ice) on top of a viscous, light fluid (gas) as shown in fig. 1. The high viscosity of the light fluid has a stabilizing effect on short-wavelength RT modes. Externally applied magnetic fields, on the order of a few to tens of tesla initially, have recently been found to be the most promising for mitigating mix in an ICF target [14] in addition to the other known benefits of alpha confinement [15] and heat loss reduction [16]. Chandrasekhar's classical work [17] has shown that magnetic fields can stabilize short-wavelength RT modes. What is particularly encouraging for ICF applications is that significant stabilization can be achieved at a magnetic-field strength that is still weak compared with the fluid energy density, *i.e.* a high-beta ICF target. Furthermore, the field line is naturally aligned to the mix interface by the stretch-and-fold magnetohydrodynamic (MHD) dynamo [14,18]. In addition to limiting the growth of Σ, magnetic fields also reduce the electron thermal conductivity across the mix interface due to electron magnetization, $\kappa_{\perp e} \ll \kappa_e$.

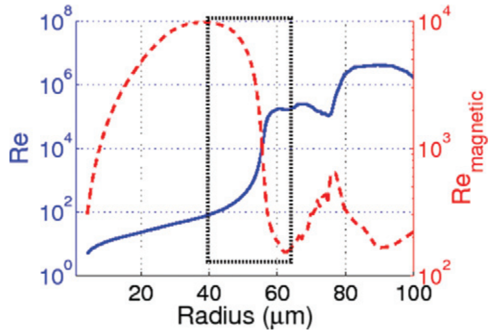

Fig. 1: (Colour on-line) Reynold's number (blue solid line) and magnetic Reynold's number (red dashed line) as a function of radius from the HELIOS-CR code [19] at peak compression.

The primary purpose of this letter is to elucidate the complementary role of the magnetic, viscous, and ablative stabilization in mitigating hydrodynamic mix at the gas-ice interface. This distinguishes the current work from the previous ones that have examined these stabilization mechanisms in isolation for ICF applications. Achieving our primary objective requires the resolution of an intrinsic competition between ablative flow due to the heat deposited at the fuel ice and magnetic insulation that inhibits hot-spot heat loss. In order to understand the complementary and competing roles, it is noted that magnetic stabilization of RTI, which is an interchange mode, occurs due to the energy required for field line bending. This implies that the magnetic stabilization effect only applies to RT modes with a wave vector $\mathbf{k}$ that is parallel to $\mathbf{B}$, *i.e.* $\mathbf{k} \times \mathbf{B} = 0$. The RTI with $\mathbf{k} \cdot \mathbf{B} = 0$ does not involve line bending so it remains unstable as predicted by hydrodynamics. The nonlinear evolution has been found to generate highly anisotropic RTI turbulence in three dimensions for astrophysical applications [20]. In ICF applications, the aim is to mitigate mix at the onset of the instability, hence one finds that ablative stabilization can play a complementary role as it applies to RTI of a $\mathbf{k}$ in either direction. Lobatchev and Betti [12] have demonstrated that the growth rate of RTI in the presence of ablative flow is quantitatively given by

$$\gamma = 0.9\sqrt{\frac{k\langle g\rangle}{1 + k\langle L_m\rangle}} - 1.4k\langle V_a\rangle. \quad (2)$$

The stabilizing effect of a smooth density gradient enters through the mass density gradient length scale, $L_m \equiv \rho/\rho'$, with ρ' defined as the radial derivative of ρ. The wave number is defined as $k = l/R_{hs}$ with the mode number l, and it becomes large for a given l as the hot spot is compressed. The ablative flow, V_a, acts to reduce the growth rate so that a higher ablation flow leads to a stronger stabilization of the RTI at the gas-ice interface. The competition between magnetic and ablative stabilization is due to

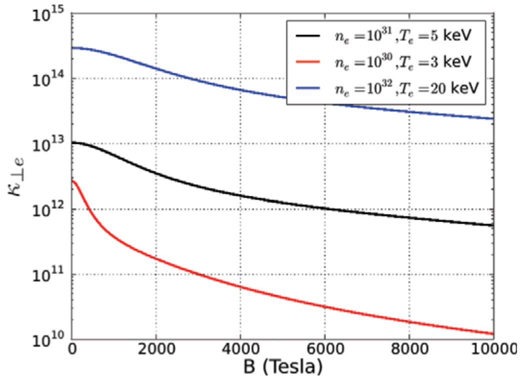

Fig. 2: (Colour on-line) $\kappa_{\perp e}$ as a function of B-field strength for three sets of ICF relevant n and T_e.

the fact that the magnitude of V_a is directly proportional to the heat flux being transferred from the hot spot to the fuel ice layer [21],

$$q_\perp = -\kappa_\perp \frac{\mathrm{d}T}{\mathrm{d}r} = \frac{5}{2} P_{hs} V_b, \tag{3}$$

where the blow-off speed is related to ablation flow via the mass continuity equation $\rho_a V_a = \rho_b V_b$. Using the isobaric condition as in Betti *et al.* [21], $P_{hs} = P_b = n_b k_B T_b$, one finds that the ablation speed is directly proportional to the heat flux

$$v_a = \frac{2}{5} \frac{q_\perp}{P_{hs}} \frac{1+A}{1-A} \tag{4}$$

with the Atwood number $A \equiv (n_b - n_a)/(n_b + n_a)$. Electron magnetization by a magnetic field that is aligned with the mix interface can cause a significant reduction in $\kappa_\perp$ [22],

$$\kappa_{\perp e} = \frac{k_B n_e k_B T_e \tau_e}{m_e} \frac{4.664(\omega_{ce}\tau_e)^2 + 11.92}{(\omega_{ce}\tau_e)^4 + 14.79(\omega_{ce}\tau_e)^2 + 3.7703},$$

where n_e is the electron number density, T_e is the electron temperature, τ_e is the electron-electron collision time, and ω_{ce} is the electron cyclotron frequency. The degree of electron magnetization is given by

$$\omega_{ce}\tau_e = \frac{eB}{m_e} \frac{12\pi^{3/2}\epsilon_0^2\sqrt{m_e}(k_B T_e)^{3/2}}{n_e e^4 \ln\Lambda}. \tag{5}$$

For strong electron magnetization, $\omega_{ce}\tau_e \sim O(10)$, $k_{\perp e}$ can be more than two orders of magnitude smaller than κ_e of an unmagnetized plasma in the ICF parameter regime, as seen from fig. 2. For an easily accessible magnetic field of thousands of tesla, $\kappa_{\perp e}$ is around 10 times smaller than the Spitzer conductivity. For comparable $\mathrm{d}T/\mathrm{d}r$ and hot-spot pressure P_{hs}, this implies a drop of 10 times for the ablation flow V_a. In reality, $\mathrm{d}T/\mathrm{d}r$ tends to be larger as $\kappa_\perp$ is reduced, and the hot-spot pressure also tends to be higher (see the online supplemental materials in ref. [23]). The net effect is still a reduced V_a but it is not linearly proportional to the reduction in $\kappa_\perp$. In any case, magnetic insulation does impede ablative stabilization. The key question is to find a balance in which adequate thermal loss reduction is achieved while the RTI with **k** perpendicular to **B** is still mitigated by ablative stabilization.

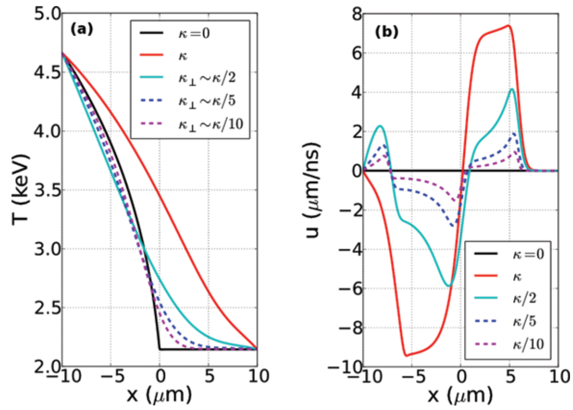

Fig. 3: (Colour on-line) Plots of temperature (a) and velocity (b) to illustrate ablation of the ice layer into the hot spot due to thermal conduction. Note that the reduced-thermal-conductivity case (factor of 5 reduction due to magnetic fields) has a steeper gradient.

Unlike ablative stabilization, which comes at the expense of the hot-spot mass gain and hence temperature cooling, the hot-spot viscous stabilization can reinforce the magnetic stabilization for modes with $\mathbf{k} \parallel \mathbf{B}$ and complement the magnetic stabilization for modes with $\mathbf{k} \perp \mathbf{B}$ without the side effect of cooling the hot spot. It must be noted that by itself, the hot-spot viscous stabilization is the least effective of the three, so it can only play a supplemental role in the overall mix mitigation strategy. Since this stabilization mechanism hinges on a high ion temperature on the hot-spot side of the gas-ice interface, it would benefit from the mix-interface–aligned magnetic field that inhibits thermal loss.

The complementary role of the three stabilization mechanisms for RTI at the gas-ice interface in the ICF parameter regime is quantified here. To illustrate the essential physics, the spherical target is unfolded to 2-dimensional (2D) planar geometry with the gas-ice interface at $y = 0$ for simplicity. As noted in the preceding text, RT in the presence of a magnetic field takes on a distinctly anisotropic character with respect to the magnetic field. This allows us to judiciously use 2D (radial and magnetic-field direction) simulations to study the magnetic stabilization of RT for a wave vector parallel to the magnetic field, and another set of 2D simulations (radial and perpendicular to the magnetic-field direction) to elucidate the complementary role of the ablative stabilization of RT with wave vector perpendicular to the magnetic field. It is this geometrical separation of the RT physics by the complementary roles of magnetic and ablative/viscous stabilization that allows insightful 2D simulations which can inform the 3D dynamics in a real target. The domain size in x is chosen to approximate the circumference at peak compression $\sim 200\,\mu$m across which the multimode

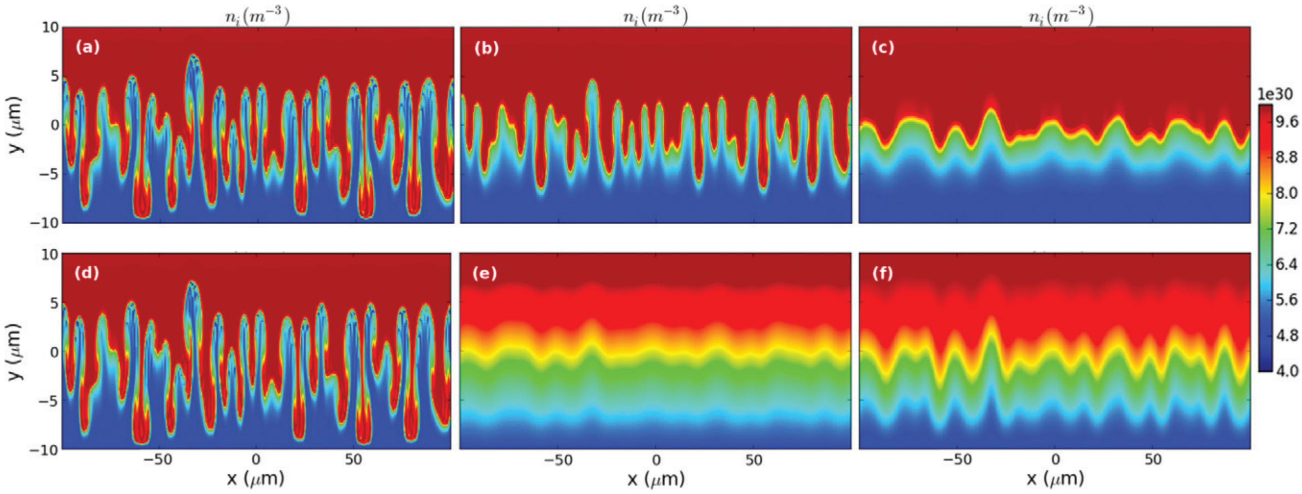

Fig. 4: (Colour on-line) Plots of density for the Euler equations after 2.8 ns with no heat flux (a), for the Navier-Stokes equations with no heat flux but disparate *Re* profile (b), for the MHD equations with no heat flux but with an in-plane B-field for the magnetic stabilization of RTI (c), for the MHD equations with a magnetic field normal to the x-y plane (d), for the MHD equations with a reduced perpendicular heat flux due to the out-of-plane B-field such that $\kappa_0/\kappa_\perp \sim 10$ (e), with a $\kappa_0/\kappa_\perp \sim 20$ (f).

perturbation is applied as in refs. [23,24]. The domain size in y is chosen to be smaller than the hot-spot radius. To model the conductive heat flow for ablative stabilization, the hot spot is set up with a temperature profile that satisfies $\kappa_e \frac{\mathrm{d}T}{\mathrm{d}y} = q_0 = \text{const}$, with electron thermal conductivity $\kappa_e \sim T^{5/2}$. The hot-spot temperature profile then matches the constant temperature of the cold fuel ice, T_c, at $y = 0$. This is shown in fig. 3(a) as a black line. With a simulated uniform gravity, g, that is representative of the capsule implosion, the density profile is found from the force balance with $p = (1 + 1/Z_i)n_e k_B T$,

$$\frac{\mathrm{d}p}{\mathrm{d}y} = \frac{n_e}{Z_i} m_i g \rightarrow \frac{\mathrm{d}\ln n_e}{\mathrm{d}y} = \frac{m_i g}{(1+Z_i)k_B T} - \frac{\mathrm{d}\ln(k_B T)}{\mathrm{d}y}.$$

To model the energy source of compressional heating in a spherical implosion that sustains the ablative flow at the gas-ice interface, a heat flux is introduced through the boundary at $y = -L$ by holding T fixed there. When κ_e becomes small at the gas-ice interface due to the $T_e^{5/2}$ dependence, the heat flow, q_0, directly sets the ablation speed at the evolving gas-ice interface, as shown in fig. 3. To be consistent with ICF implosions, this ablation speed is matched to that typically observed in 1D spherical implosion simulations of ignition-type targets in HELIOS-CR. The value is found to be around 13–25 μm/ns, consistent with Betti *et al.* [25].

Simulations are performed using the same initial conditions but with each of the RTI stabilization mechanisms implemented in isolation and in combination. The results are shown as density contours in fig. 4 where all contours are plotted at $t = 2.8$ ns. Panel (a) is the conventional inviscid hydrodynamic simulation without thermal conduction and magnetic fields, and is shown to produce a robust RTI solution forming a large mixing layer. The case with hot-spot ion viscous stabilization is shown in panel (b), with a Reynolds number profile similar to fig. 1. Despite the Reynolds number in the ice being turbulent, $Re \sim 10^4$, the laminar $Re \sim 10^2$ in the gas mostly regularizes the fine-scale RTI and slows RTI growth.

Figure 4(c) presents the solution with a large external in-plane magnetic field as studied in ref. [14] but for the new initial condition profile from fig. 3. It is important to note that a 1000 tesla field at the onset of deceleration corresponds to a 10 tesla initial seed field after the target is compressed by a factor of ten. Such compressional gain in field strength has been observed in laboratory experiments [16,26–28]. The ~ 1000 tesla in-plane magnetic field at the onset of deceleration, which is used as the initial condition for our simulations, grows due to the MHD dynamo [29–31] and damps short-wavelength RTI significantly as expected [17,32,33]. Furthermore, the resulting large in-plane magnetic fields slow the growth of long-wavelength modes. As shown in ref. [14], the plasma $\beta \sim O(10^2)$ (ratio of plasma pressure to magnetic pressure) when the magnetic fields affect the dynamics of the RTI. The plot shows that the mixing layer length is greatly reduced with only longer-wavelength modes growing slowly.

As previously noted, the magnetic field does not have a stabilizing effect for RTI modes with $\mathbf{k} \cdot \mathbf{B} = 0$, because such modes do not induce field line bending. This is verified in fig. 4(d) where a similarly strong magnetic field normal to the x-y plane does not impede the RTI growth at all. Here, the ablative stabilization, which has the undesirable property of increasing the hot-spot mass and lowering its temperature but is independent of the direction of $\mathbf{k}$, can have a complementary role in reducing RT mix. Since the ablation flow speed is directly proportional to the heat flow, there is also a competition between magnetic and ablative stabilization because an interface-aligned magnetic field impedes the heat flow across the interface, and hence reduces v_a and the effectiveness of ablative stabilization. To resolve this competition, 2D simulations are performed with magnetic field normal to the x-y plane to introduce a $\kappa_\perp$ that is many times smaller than the unmagnetized value κ_0. It is important to note that the interface alignment of magnetic fields via MHD dynamo is only effective around the interface, which is stretched by the RTI. Furthermore, the magnetic field inside the hot spot is both weaker (since there is less stretching) and not properly aligned, so the effective radial thermal conductivity is still about κ_0. Hence, the simulation domain $[-L, L]$ is chosen such that L is smaller than the hot-spot size. For the same reason, the plasma temperature is held fixed at the two boundaries since an insulating layer would act as a transport barrier and maintain a high temperature at $y = -L$ (hence a smaller temperature gradient across the remaining part of the hot spot) in order to be consistent with the reduced hot-spot thermal energy loss.

With this simulation setup, the competition between magnetic insulation and ablative stabilization can be resolved by varying B_z and hence $\kappa_\perp$ while holding fixed the plasma temperature at $y = -L$ and $y = L$. Figure 4(e) shows the case of $\kappa_\perp/\kappa_0 = 0.1$, where, despite a decrease in v_a, the ablative stabilization reduces the RTI growth significantly. It is important to note that the density gradient is significantly reduced compared with the unmagnetized plasma because $\kappa_\perp \sim T^{-1/2}$ as opposed to $\kappa_0 \sim T^{5/2}$, which produces a more gradual variation in temperature and hence density for an isobaric plasma.

As expected, if $\kappa_\perp$ is further decreased by a stronger B_z, the ablative stabilization becomes less effective as demonstrated in fig. 4(f) for $\kappa_\perp/\kappa_0 \approx 0.05$. The RTI mode growth is still significantly slower than that of the unmagnetized case, fig. 4(a), but appreciably stronger than the $\kappa_\perp/\kappa_0 \approx 0.1$ case, fig. 4(e). In the limit of a really small $\kappa_\perp$ such that $\kappa_\perp/\kappa_0 < 0.01$, the RTI growth essentially recovers the case in panel (a). This is a limiting case, from fig. 2, that is only relevant for sub-ignition targets, which have too low a density and a temperature to be of a practical concern.

Figure 5 shows the effect of isolating thermal conduction on the RT growth and the ablation front. Note that without magnetic fields, the thermal conduction is very large and for the same time of 2.8 ns as in fig. 4, the ablation front has penetrated significantly into the ice without RT development in the specific case considered. While this has the effect of mitigating the RT mix almost completely, it does so at the expense of significant hot-spot mass gain and associated hot-spot cooling, which can be a detrimental factor for an implosion platform that is at the marginal ignition boundary.

It is important to note that the findings reported here are from a physics study, which is greatly facilitated by a simplifying planar geometry. The study is the first to establish the synergistic role of three distinct physical mechanisms, namely magnetic, ablative, and viscous stabilization, in mitigating mix for ICF. This hopefully helps in motivating the actual spherical target design towards fielding an implosion experiment. Specifically our physics findings suggest that mitigating the RT mix in a spherical target is a two-step process that trades long-wavelength RT of modestly increased mix interfacial area for RT turbulence which can have enormously amplified mix interfacial area. The first step is the rapid development of a long-wavelength RT mode that amplifies and aligns a magnetic field with the gas-ice interface. This crucially depends on the stretch-and-fold MHD dynamo mechanism associated with the long-wavelength RT that aligns the magnetic field with the mix interface for an initial magnetic field that intercepts the gas-ice interface at a large angle. Once such electron-magnetizing and interface-aligned field is in place, the second step is the search for a balance among reduced ablative stabilization, anisotropic magnetic stabilization, and the ion viscous stabilization which relies on a high-temperature hot spot. Our simulation results indicate the existence of a parameter regime for such a synergistic effect of three separate physical mechanisms. The fact that the initial anisotropic ablation, due to a misaligned magnetic field with respect to the mix interface in a spherical target, can promote the initial growth of long-wavelength RT, is a physics subtlety that actually helps expedite the dynamic alignment process.

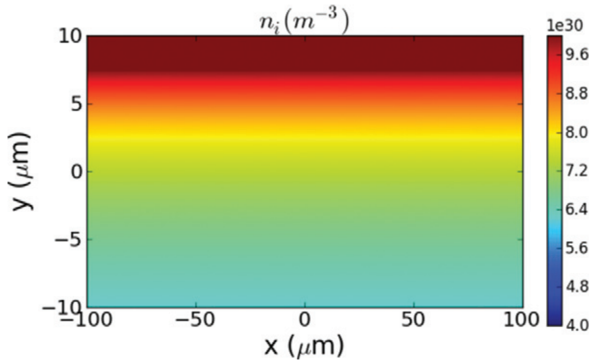

Fig. 5: (Colour on-line) Density evolution at 2.8 ns for the same scale as shown in fig. 4 in the presence of thermal conduction only without any effect of magnetic fields and viscosity. Note that the RT does not get a chance to develop at all; however, there is a significant amount of mass ablated from the ice into the hot spot. This can be seen from the location of the ablation front here that is well into the ice layer.

In summary, magnetic and ablative stabilization have been shown to work in tandem to mitigate the RTI growth at the gas-ice interface for **k** both parallel and perpendicular to **B**. Once the ignition temperature is reached, the hot-spot ion viscous stabilization can also be appreciable. It is emphasized that the magnetic stabilization is particularly useful because, in addition to stabilizing the modes with **k** parallel to **B**, it also reduces the thermal loss across the gas-ice interface by aligning itself, via MHD dynamo, to the mix interface. The magnetic insulation does reduce the heat flow into the ice and results in a smaller ablation flow. But for parameters of ignition interest, where $\kappa_\perp/\kappa_0 \sim 0.1$, the ablation flow is still significant enough to drastically reduce the RTI growth of modes with $\mathbf{k}\cdot\mathbf{B} = 0$. This is also aided by the fact that the different scaling of $\kappa_\perp$ with respect to T naturally produces a weaker gradient in T and hence density n, which has long been known to be stabilizing [12,34] for a large L_m in eq. (2).

* * *

This research was supported by the U.S. Department of Energy at Los Alamos National Laboratory. The authors wish to acknowledge the use of the WARPX code which was developed at the University of Washington. All simulations in this paper were performed using the Los Alamos National Laboratory Institutional Computing and Turquoise network clusters.

REFERENCES

[1] Hurricane O. A., Callahan D. A., Casey D. T., Celliers P. M., Cerjan C., Dewald E. L., Dittrich T. R., Döppner T., Hinkel D. E., Berzak Hopkins L. F., Kline J. L., Le Pape S., Ma T., MacPhee A. G., Milovich J. L., Pak A., Park H.-S., Patel P. K., Remington B. A., Salmonson J. D., Springer P. T. and Tommasini R., *Nature*, **506** (2014) 343.

[2] Park H.-S., Hurricane O., Callahan D., Casey D., Dewald E., Dittrich T., Döppner T., Hinkel D., Berzak Hopkins L. F., Le Pape S., Ma T., Patel P., Remington B., Robey H., Salmonson J. and Kline J. L., *Phys. Rev. Lett.*, **112** (2014) 055001.

[3] Dittrich T., Hurricane O., Callahan D., Dewald E., Döppner T., Hinkel D., Berzak Hopkins L. F., Le Pape S., Ma T., Milovich J., Moreno J., Patel P., Park H.-S., Remington B., Salmonson J. and Kline J. L., *Phys. Rev. Lett.*, **112** (2014) 055002.

[4] Paisner J. A., Campbell E. M. and Hogan W. J., *Fusion Technol.*, **26** (1994) 755.

[5] Atzeni S. and Meyer-Ter-Vehn J., *The Physics of Inertial Fusion* (Oxford University Press, Inc.) 2004.

[6] Edwards M. J., Lindl J. D., Spears B. K., Weber S. V. *et al.*, *Phys. Plasmas*, **18** (2011) 051003.

[7] Nuckolls J., Wood L., Thiessen A. and Zimmerman G., *Nature*, **239** (1972) 139.

[8] Anderson K. and Betti R., *Phys. Plasmas*, **11** (2004) 5.

[9] Ma T., Patel P. K., Izumi N., Springer P. T. *et al.*, *Phys. Rev. Lett.*, **111** (2013) 085004.

[10] Hammel B., Haan S. W., Clark D. S., Edwards M. J. *et al.*, *HEDP*, **6** (2010) 171.

[11] Hammel B., Scott H. A., Regan S. P., Cerjan C. *et al.*, *Phys. Plasmas*, **18** (2011) 056310.

[12] Lobatchev V. and Betti R., *Phys. Rev. Lett.*, **85** (2000) 4522.

[13] Schiavi A. and Atzeni S., *Phys. Plasmas*, **14** (2007) 070701.

[14] Srinivasan B. and Tang X.-Z., *Phys. Plasmas*, **20** (2013) 056307.

[15] Perkins L. J., Logan B. G., Zimmerman G. B. and Werner C. J., *Phys. Plasmas*, **20** (2013) 072708.

[16] Chang P. Y., Fiksel G., Hohenberger M., Knauer J. P., Betti R., Marshall F. J., Meyerhofer D. D., Seguin F. H. and Petrasso R. D., *Phys. Rev. Lett.*, **107** (2011) 035006.

[17] Chandrasekhar S., *Hydrodynamic and Hydromagnetic Stability* (Oxford University Press, Inc.) 1961.

[18] Tang X. Z. and Boozer A. H., *Phys. Plasmas*, **7** (2000) 1113.

[19] MacFarlane J. J., Golovkin I. E. and Woodruff P. R., Technical Report, Prism Computational Sciences (2005).

[20] Stone J. M. and Gardiner T., *Astrophys. J.*, **671** (2007) 1726.

[21] Betti R., Anderson K., Goncharov V. N., Mccrory R. L., Meyerhofer D. D., Skupsky S. and Town R. P. J., *Phys. Plasmas*, **9** (2002) 2277.

[22] Braginskii S. I., *Rev. Plasma Phys.*, **1** (1965) 205.

[23] Srinivasan B., Dimonte G. and Tang X.-Z., *Phys. Rev. Lett.*, **108** (2012) 165002.

[24] Srinivasan B. and Tang X.-Z., *Phys. Plasmas*, **19** (2012) 082703.

[25] Betti R., Umansy M., Lobatchev V., Goncharov V. N. and Mccrory R. L., *Phys. Plasmas*, **8** (2001) 5257.

[26] Knauer J. P., Gotchev O. V., Chang P. Y., Meyerhofer D. D., Polomarov O., Betti R., Frenje J. A., Li C. K., Manuel M. J. E., Petrasso R. D., Rygg J. R. and Seguin F. H., *Phys. Plasmas*, **17** (2010).

[27] Yoneda H., Namiki T., Nishida A., Kodama R., Sakawa Y., Kuramitsu Y., Morita T., Nishio K. and Ide T., *Phys. Rev. Lett.*, **109** (2012) 125004.

[28] Fujioka S., Zhang Z., Yamamoto N., Ohira S., Fujii Y., Ishihara K., Johzaki T., Sunahara A., Arikawa Y., Shigemori K., Hironaka Y., Sakawa Y., Nakata Y., Kawanaka J., Nagatomo H., Shiraga H., Miyanaga N., Norimatsu T., Nishimura H. and Azechi H., *Plasma Phys. Control. Fusion*, **54** (2012) 124042.

[29] Alfvén H., *Tellus*, **2** (1950) 74.

[30] Vainshtein S. I. and Zel'dovich Y. B., *Sov. Phys. Usp.*, **15** (1972) 159.

[31] Childress S. and Gilbert A., *Stretch, Twist, Fold: The Fast Dynamo* (Springer) 1995.

[32] Jun B., Norman M. and Stone J., *Astrophys. J.*, **453** (1995) 332.

[33] Stone J. M. and Gardiner T., *Phys. Fluids*, **19** (2007) 094104.

[34] Lindl J. D., *Inertial Confinement Fusion* (Springer, New York) 1998.